J. Fluid Mech. (1994), *vol.* 269, *pp.* 247–264

Instability of strongly nonlinear waves in vortex flows

By A. KRIBUS[1] AND S. LEIBOVICH[2]

[1]Weizmann Institute of Science, Rehovot, Israel

[2]Cornell University, Ithaca, NY 14853–7501, USA

(Received 21 July 1992 and in revised form 17 December 1993)

Weakly nonlinear descriptions of axisymmetric cnoidal and solitary waves in vortices recently have been shown to have strongly nonlinear counterparts. The linear stability of these strongly nonlinear waves to three-dimensional perturbations is studied, motivated by the problem of vortex breakdown in open flows. The basic axisymmetric flow varies both radially and axially, and the linear stability problem is therefore non-separable. To regularize the generalization of a critical layer, viscosity is introduced in the perturbation problem. In the absence of the waves, the vortex flows are linearly stable. As the amplitude of a wave constituting the basic flow increases owing to variation in the level of swirl, stability is first lost to non-axisymmetric 'bending' modes. This instability occurs when the wave amplitude exceeds a critical value, provided that the Reynolds number is larger enough. The critical wave amplitudes for instability typically are large, but not large enough to create regions of closed streamlines. Examination of the most-amplified eigenvectors shows that the perturbations tend to be concentrated downstream of the maximum streamline displacement in the wave, in a position consistent with the observed three-dimensional perturbations in the interior of a bubble type of vortex breakdown.

1. Introduction

It has long been known on theoretical grounds that concentrated vortex flows with or without axial streaming are dispersive waveguides admitting propagation of waves of finite amplitude along their cores. The primary vortices upon which the waves propagate are nearly columnar, having a structure that varies slowly with distance along the axis of the vortex. Long axisymmetric waves on strictly columnar primary flows are governed by the Korteweg–de Vries (KdV) equation. Finite-amplitude wavetrains (cnoidal waves) and solitary waves are possible waves of permanent form (Benjamin 1967; Pritchard 1970; Leibovich 1970). These weakly nonlinear waves had been presumed possible also at higher amplitudes, and this has recently been verified by Leibovich & Kribus (1990, henceforth referred to as L&K). The studies cited, while fundamental in nature and having a variety of applications, were all motivated by the goal of better understanding of the phenomenon of vortex breakdown. This paper, which investigates the three-dimensional *stability* of the axisymmetric waves, follows in the same path and has the same goals.

Solitary waves and cnoidal wavetrains found from the Korteweg–de Vries equation are stable within the KdV framework, as shown by Benjamin (1972, 1974). The weakly nonlinear theory leading to the KdV equation is a valid asymptotic representation of solutions of the Euler equations for axisymmetric small-amplitude long waves. A

declaration of stability that follows from the KdV representation is not valid for the large-amplitude waves that exist within the larger framework of the axisymmetric Euler equations. Furthermore, stability to three-dimensional perturbations cannot be established within the KdV framework, no matter how small the waves. There is consequently a need for a more complete discussion of stability, and this is the objective of this paper.

An earlier attempt to examine the stability problem by Mac Giolla Mhuiris (1986*a*, *b*) was inconclusive. He examined the stability of the KdV cnoidal wave to three-dimensional perturbations, but his numerical method did not permit sufficient spatial resolution to detect unstable modes. Considerable effort was made in the course of our research to devise numerical procedures for very large eigenvalue problems which would permit adequate spatial resolution. Discussion of the methods used appears in Kribus (1991), and a brief account is given in the Appendix.

It is only sensible to consider the stability of basic flows consisting of finite-amplitude waves when the primary columnar flow is stable, and we therefore restrict attention to such cases. The numerical evidence reported here indicates that the large-amplitude axisymmetric waves are indeed stable to axisymmetric perturbations, as the small-amplitude KdV analysis suggests. They are also stable to three-dimensional disturbances provided the waves have moderate amplitudes. For sufficiently large amplitudes, the waves first lose stability to three-dimensional 'bending' or 'sloshing' mode (azimuthal wavenumber $= \pm 1$) instabilities. This, and the form of the unstable eigenmodes, are consistent with the non-axisymmetric features observed in vortex breakdown experiments. As the wave amplitude is increased, the flow on the axis is decelerated beneath the wave crest, and local flow reversal occurs when the wave amplitude exceeds a particular value. The critical wave amplitude for instability to bending modes found here is reached before the wave is large enough to cause flow reversal.

We set out in §2 the basic flows in L&K whose stability are to be examined. The stability problem is posed in §3, stability results for columnar flows are reported in §4, results for waves are reported in §5, and the paper is summarized in §6.

2. Base flows

The domain of interest is an infinitely long tube of constant circular cross-section, and the analysis is carried out in a cylindrical (r, θ, z) coordinate system, with velocity vector (u, v, w).

Any 'columnar' flow (by definition depending only on radial distance from an axis of symmetry) is an exact solution of the Euler equations. The basic flows tested for stability in this paper are nonlinear waves which may propagate on columnar vortices. To investigate stability, a numerical treatment is needed, and one must select a concrete form for the underlying columnar state, which we call the primary columnar flow. The examples treated in L&K are members of a multiple-parameter family:

$$W(r) = W_1 + W_2 \mathrm{e}^{-\beta r^2}, \tag{1a}$$

$$rV(r) = \lambda(1 - \mathrm{e}^{-\alpha r^2}), \tag{1b}$$

with the particular choice $W_2 = 0$, and a velocity scale selected to make $W_1 = 1$. This reduces (1) to a two-parameter family sometimes called the Burgers–Rott vortex. The same two-parameter family of primary flows is adopted here. The complete forms (1) were used by Garg & Leibovich (1979), and by Maxworthy, Hopfinger & Redekopp (1985) to fit their velocity measurements in flows ahead and downstream of vortex

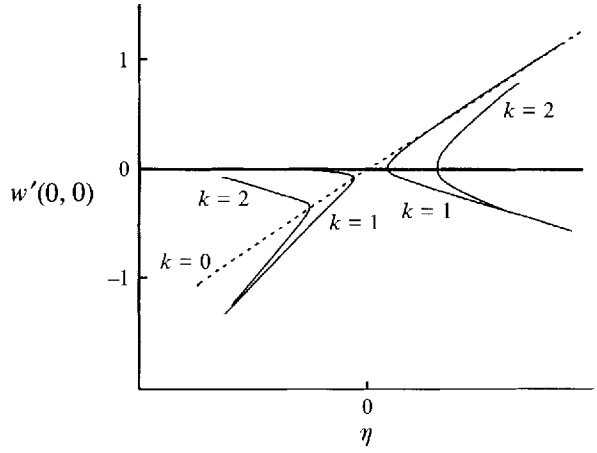

FIGURE 1. Bifurcation diagram near the principal bifurcation point. $k = 0$: columnar solution; $k = 1$: wave of period L; $k = 2$: wave of period $\frac{1}{2}L$.

breakdown. It will be shown here that some of the columnar solutions bifurcating from the Burgers–Rott vortex also may be fitted accurately to the generalized exponential family (1).

Weakly nonlinear wave theory indicates that the amplitude of stationary axisymmetric waves of a fixed wavelength is related to the level of swirl. L&K constructed strongly nonlinear waves by the continuation of these weakly nonlinear steady solutions. Continuation was carried out by considering a one-parameter family of columnar primary flows, with the vortex circulation as the control parameter. More than one wave branch is possible for a specific primary flow. In addition, at a particular value of the circulation, a second steady columnar flow branches from the primary one (these are the 'conjugate flows', as discussed by Benjamin 1962). The amplitude of the waves is found to be an increasing function of the departure of the circulation from a discrete set of branching values.

2.1. *Bifurcations from the primary flow*

Fully nonlinear inviscid perturbations to the primary columnar flow can be found. Solutions periodic in z depend on three parameters: α, describing the radial rate of decay of axial vorticity; Λ, the square of the dimensionless circulation; and the period, L, of the motion in the z-direction. Holding α and L fixed, and treating Λ as the bifurcation parameter, various solutions branch from the primary columnar flow at discrete values of Λ. The kinds of solutions found are conveniently summarized in a bifurcation diagram. Figure 1 is a composite of typical bifurcation diagrams with examples of three solutions that branch from the primary vortex. Near its bifurcation point, each branch is a periodic function of $2k\pi z/L$. In the figure, branches are identified by axial wavenumber k: a columnar branch ($k = 0$) and branches of the fundamental ($k = 1$) and first-harmonic ($k = 2$) wavy solutions are shown. All values of α and L produce qualitatively similar diagrams, the main difference being a rapid decrease in the separation between the curves for the columnar branch and the first wavy branch with increasing α. The upper and lower branches at each fixed $k > 0$ correspond to identical flows, but shifted axially as explained in L&K.

To identify the location of specific points on the bifurcation diagram, we use a parameter

$$\eta \equiv (\Lambda/\mu) - 1$$

that measures the relative distance from μ, the point at which the branch labelled $k = 0$ on figure 1 bifurcates from the primary columnar flow. The $k = 0$ branch is also columnar, and we will call it the 'secondary columnar flow'. Other columnar flows branch from the primary one, but they are all centrifugally unstable, and we therefore consider them physically irrelevant.

The extreme value (regardless of sign) of the perturbation axial velocity w', which usually occurs at $r = z = 0$, is used as a measure of the perturbation size (see L&K for some cases where the extreme perturbation velocity is found off the axis). The locations of bifurcation points for several values of L and α are given by L&K.

2.2. *Columnar branches*

For $\eta < 0$, the secondary columnar branch shows a developing wake-like axial velocity profile as the swirl parameter A is decreased from the branch point μ, as may be seen in figure 2 of L&K. The swirl velocity is distorted as well, with the peak swirl moving outwards. On the $\eta > 0$ side of the principal branch, the axial velocity profiles are jet-like, and the peak swirl moves towards the axis, as may be seen from figure 3 of L&K. The velocity profiles can be fitted to the exponential profiles (1). Faler & Leibovich (1977) were able to fit their measured velocity profiles to a similar function, with $\beta = \alpha$. The values of β found here differ from α, so that (1) defines a wider category of 'exponential profiles', similar to those used by Maxworthy *et al.* (1985). We fitted the model (1) to the computed velocity profiles using a Chi-Square algorithm. The fit is shown by Kribus (1991) to be quantitatively excellent for the range $-0.5 \leqslant \eta \leqslant 1.1$, and to be qualitatively good up to $\eta = 1.5$.

The values of the fit parameters vary smoothly with η, as shown in Kribus (1991), who is able to obtain an explicit model for $W(r;\eta)$ in the form of equation (1):

$$\left.\begin{aligned} W_1(\eta) &= 0.975(\eta+1)^{-0.078}, \\ W_2(\eta) &= 2.45\eta - 0.268\eta^2, \\ \beta(\eta) &= 31.2 + 18.2\eta - 3.84\eta^2. \end{aligned}\right\} \tag{2}$$

The azimuthal velocity profiles do not need to be fitted separately, since the circulation is a function of the Stokes streamfunction $\psi(r,z;\eta)$, so that ψ can be computed from the axial velocity model. For a given η, we have for the secondary columnar flow

$$\psi(r,z;\eta) = \tfrac{1}{2}W_1(\eta)\,r^2 + \frac{W_2(\eta)}{2\beta(\eta)}\,\mathrm{e}^{-\beta(\eta)\,r^2},$$

$$rV(r;\eta) = \lambda(1-\mathrm{e}^{-2\alpha\psi(r;\eta)}).$$

2.3. *Periodic wavetrains*

The fully nonlinear periodic wavetrains calculated by L&K are continuations of weakly nonlinear solutions. For large L, these weakly nonlinear wavetrains are the cnoidal waves previously derived by Benjamin (1967), and also obtained by Pritchard (1970) and by Leibovich (1970). The form of the streamfunction in the weakly nonlinear approximations is

$$\psi(r,z) = \phi(r)\,A(z), \quad A(z) = a\,\mathrm{cn}^2(bz\,|\,\bar{k}) + c, \tag{3}$$

where $\mathrm{cn}(x)$ is one of the Jacobi elliptic function, $\bar{k}$ is the elliptic modulus of the cn function, and a, b and c are functionals of the primary columnar flow (see Kribus 1991). The amplitude function $\phi(r)$ is determined by a linear eigenvalue problem (where the eigenvalue has already been introduced as μ). For details, see L&K.

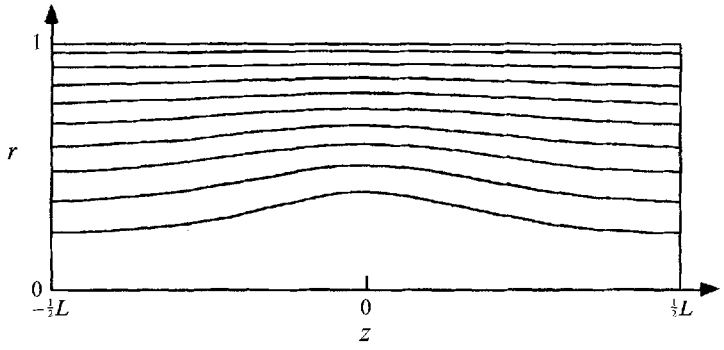

FIGURE 2. Streamlines in the (r, z)-plane for the $\eta = 0.1$ wave solution on the $\alpha = 3$, $L = 2$, $k = 1$ branch.

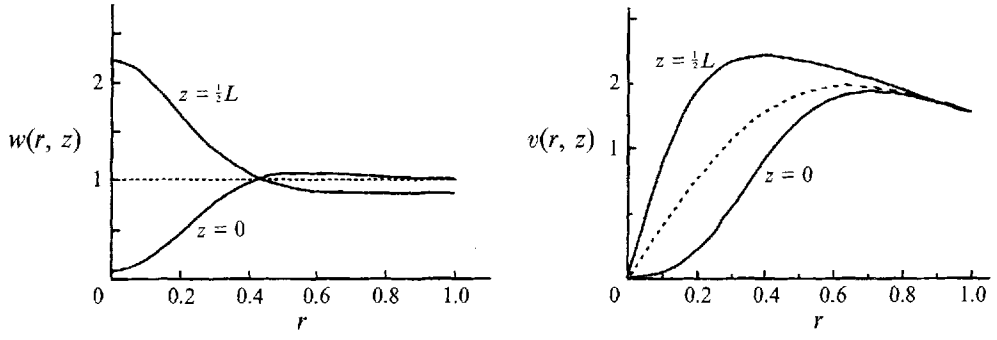

FIGURE 3. Axial and azimuthal velocity profiles for $\alpha = 3$, $L = 2$, $k = 1$, $\eta = 0.1$ flow at the wave centre $z = 0$ and the trough $z = \frac{1}{2}L$. Dotted line: $\eta = 0$ profile.

In a computation with a large fixed axial length L and a fixed value of Λ near μ we should expect then to find several types of solutions, besides the original primary vortex: the secondary columnar flow, which branches off at μ; periodic cnoidal waves with period L and higher harmonics which branch at a sequence of points with $\Lambda > \mu$; and, as $L \to \infty$, solitary waves which are superposed on either the primary or secondary branch, depending on the sign of η. This expectation is confirmed in L&K, where some of these small-amplitude waves are continued to finite amplitude.

Typical streamlines for an axially varying solution on the $k = 1$ branch are shown in figure 2, and corresponding velocity profiles are presented in figure 3. L&K found that as the wave increases in amplitude, the deceleration of the flow near the axis is more apparent, and eventually a recirculation region appears. The axial variations and velocity distributions of the $\eta < 0$ solutions are qualitatively similar to those of the $\eta > 0$ branches. One main difference is the crest region of the wave, which approaches the primary branch for $\eta < 0$ and the conjugate branch for $\eta > 0$. This difference can also be inferred from figure 1. As shown in L&K, the fully nonlinear periodic solutions resemble the weakly nonlinear cnoidal wave solutions even though the perturbation is not small.

Several solutions of the Navier–Stokes equations in the same geometry are available, and have features resembling the inviscid wavy motions. Most computations are at low Reynolds number (Re), and are not suitable for direct comparison with inviscid solutions. Salas & Kuruvila (1989) and Beran (1987) present solutions up to $Re = 1800$ and 9977, respectively, for several values of the swirl and large L. They found that

increasing Re initially increases the wave amplitude. At larger values, the wave amplitude saturates and more waves appear downstream of the first at regular intervals, with progressively more uniform amplitudes. As Beran notes, the viscous solution approaches an inviscid periodic wavetrain for large Re. The effect of increasing the swirl is to increase the wave amplitude, corresponding to the $\eta > 0$ branches of the inviscid wavetrains. The details of the flow inside the viscous wave region are very different from the inviscid solutions, however, this aspect is further discussed in Kribus (1991).

Inviscid solutions for different primary columnar flows found by other investigators (Ts'asan 1986; Hafez, Kuruvila & Salas 1986) are qualitatively the same as the cases examined here; we therefore believe it likely that the results presented in L&K are generic to rotating axisymmetric flows, rather than specific to our choice of the primary columnar vortex. The small-viscosity limit of the viscous solutions also agrees in general form, if not in details, with the present invicid solutions.

3. The linear stability problem

The base flows considered here are steady solutions of the Euler equations. We include the viscous terms in the linear stability problem, however, as a way to resolve possible (generalized) 'critical-layer' singularities. Perturbations are assumed with a small but finite physical viscosity, and we study the stability characteristics as the viscosity is decreased. This would resolve inviscid modes that are the limit of viscous modes as $\nu \to 0$.

To this end, consider a flow with a steady, inviscid solution $\boldsymbol{U}$ as initial condition and a large Reynolds number (based on a measure of $|\boldsymbol{U}|$). A small perturbation $\boldsymbol{u}$ to this flow will initially evolve according to the linearized equation

$$\frac{\partial \boldsymbol{u}}{\partial t} = -\boldsymbol{u}\cdot\nabla\boldsymbol{U} - \boldsymbol{U}\cdot\nabla\boldsymbol{u} - \nabla p + Re^{-1}\nabla^2\boldsymbol{u} + Re^{-1}\nabla^2\boldsymbol{U}. \tag{4}$$

The flow will evolve slowly due to viscosity even if no perturbations are present at time $t = 0$, and this evolution is forced by the inhomogeneous term representing the viscous force generated by $\boldsymbol{U}$. In addition to this evolution, if any perturbations to $\boldsymbol{U}$ are present then the evolution may differ, and this is especially so if the base flow $\boldsymbol{U}$ is subject to instability. We wish to distinguish the relative rates of change for $Re \gg 1$ due to instabilities and the growth rate due to direct viscous development of $\boldsymbol{U}$. The rate of change due to the presence of the small perturbation having initial amplitude measured by ϵ is $\epsilon\sigma_r$, where σ_r is the growth rate of the leading linear mode. The rate of evolution due to direct viscous development is $O(Re^{-1})$. If $\sigma_r \gg (\epsilon Re)^{-1}$, then the evolution of the flow will be dominated by the linear instability. Otherwise, the flow is not likely to follow the growth predicted by linear theory, due to the effects of viscosity on the initial field $\boldsymbol{U}$. We will therefore describe as 'linearly unstable' only those cases for which $\sigma_r \gg (\epsilon Re)^{-1}$.

The steady, axisymmetric base flow $\boldsymbol{U}(r, z) = (U, V, W)$ does not depend on the azimuth and is periodic in the axial direction. Infinitesimal, three-dimensional perturbations $\boldsymbol{u}(r, \theta, z, t)$ satisfy the Navier–Stokes equations linearized about $\boldsymbol{U}$. The governing partial differential equations therefore have coefficients periodic in z, and therefore the stability problem may be treated by Floquet theory. In particular, we may look for solutions in the form $\boldsymbol{u}(r, \theta, z, t) = \mathrm{e}^{\mathrm{i}\kappa z}\boldsymbol{Q}(r, \theta, z, t)$, where $\boldsymbol{Q}$ is periodic in z with the same period as the base flow. We may then construct solutions in the form

$(ru, rv, rw, rp) \equiv (\alpha, \beta, \gamma, \pi)\,\mathrm{e}^{\sigma t + \mathrm{i}m\theta + \mathrm{i}\kappa z}$, where α, β, γ and π are functions of (r, z) with period L in z. Here m may be any integer, and κ may be an arbitrarily assigned real number.

Introducing this form, the linearized continuity and momentum equations are

$$\frac{\partial\alpha}{\partial r}+\frac{\mathrm{i}m\beta}{r}+\frac{\partial\gamma}{\partial z}+\mathrm{i}\kappa\gamma = 0, \tag{5a}$$

$$\begin{aligned}\sigma\alpha = {} & \frac{\partial}{\partial r}\left[-2U\alpha+\frac{1}{Re}r\frac{\partial}{\partial r}\left(\frac{\alpha}{r}\right)\right]+\frac{\partial}{\partial z}\left[-(U\gamma+W\alpha)+\frac{1}{Re}\left(\frac{\partial\alpha}{\partial z}\right)\right]\\ & -\frac{\mathrm{i}m}{r}(U\beta+V\alpha)-\mathrm{i}\kappa(U\gamma+W\alpha)+2\frac{V\beta}{r}\\ & +\frac{1}{Re}\left(-\frac{2\mathrm{i}m\beta}{r^2}-\kappa^2\alpha+2\mathrm{i}\kappa\frac{\partial\alpha}{\partial z}-(m^2+1)\frac{\alpha}{r^2}\right)-r\frac{\partial}{\partial r}\left(\frac{\pi}{r}\right),\end{aligned} \tag{5b}$$

$$\begin{aligned}\sigma\beta = {} & \frac{\partial}{\partial r}\left[-(U\beta+V\alpha)+\frac{1}{Re}r\frac{\partial}{\partial r}\left(\frac{\beta}{r}\right)\right]+\frac{\partial}{\partial z}\left[-(W\beta+V\gamma)+\frac{1}{Re}\left(\frac{\partial\beta}{\partial z}\right)\right]\\ & -2\frac{\mathrm{i}mV\beta}{r}-\mathrm{i}\kappa(W\beta+V\gamma)-\frac{U\beta+V\alpha}{r}\\ & +\frac{1}{Re}\left(\frac{2\mathrm{i}m\alpha}{r^2}-(m^2+1)\frac{\beta}{r^2}-\kappa^2\beta+2\mathrm{i}\kappa\frac{\partial\beta}{\partial z}\right)-\frac{\mathrm{i}m\pi}{r},\end{aligned} \tag{5c}$$

$$\begin{aligned}\sigma\gamma = {} & \frac{\partial}{\partial r}\left[-(U\gamma+W\alpha)+\frac{1}{Re}r\frac{\partial}{\partial r}\left(\frac{\gamma}{r}\right)\right]+\frac{\partial}{\partial z}\left[-2W\gamma+\frac{1}{Re}\left(\frac{\partial\gamma}{\partial z}\right)\right]\\ & -\frac{\mathrm{i}m(V\gamma+W\beta)}{r}-2\mathrm{i}\kappa W\gamma+\frac{1}{Re}\left(2\mathrm{i}\kappa\frac{\partial\gamma}{\partial z}-\frac{m^2\gamma}{r^2}-\kappa^2\gamma\right)-\frac{\partial\pi}{\partial z}-\mathrm{i}\kappa\pi.\end{aligned} \tag{5d}$$

The viscous term involving the base flow, $Re^{-1}\nabla^2 U$, is assumed small compared to terms of first order in the perturbation velocity, as explained above.

At the axis $r = 0$ the velocity field must be regular, leading to

$$\alpha = \beta = \gamma = \pi = 0. \tag{5e}$$

The boundary $r = 1$ is treated as a stress-free surface:

$$\alpha = \frac{\partial}{\partial r}\left(\frac{\beta}{r^2}\right) = \frac{\partial}{\partial r}\left(\frac{\gamma}{r}\right) = 0. \tag{5f}$$

The functions $(\alpha, \beta, \gamma, \pi)$ have the same fundamental period as the base flow:

$$(\alpha, \beta, \gamma, \pi)|_{(r, \frac{1}{2}L)} = (\alpha, \beta, \gamma, \pi)|_{(r, -\frac{1}{2}L)}. \tag{5g}$$

Equations (5*a–g*) form an eigenvalue problem for the complex growth rate σ. It depends on the parameters κ and m (axial and azimuthal wavenumbers) and Re (Reynolds number), and on the choice of axisymmetric base flow $\boldsymbol{U}$; the base flow, in turn, depends on the period L and (for the flows derived from the Burgers vortex) the radial scaling α.

We apply centre differences to (5) on a Cartesian grid with uniform intervals in the (r, z)-plane, to obtain a generalized matrix eigenvalue problem of the form

$$\boldsymbol{A}\boldsymbol{x} = \sigma\boldsymbol{B}\boldsymbol{x} \tag{6}$$

where the vector of unknowns is $x = (\alpha, \beta, \gamma, \pi)^T$, the velocities and pressure at the grid points. On a grid of $M \times N$ interior points, the size of x and the matrices is $4MN$. The matrices $\boldsymbol{A}$ and $\boldsymbol{B}$ are in general very sparse, and have only a few non-zero diagonals each. A more detailed description of the algebraic problem (6) may be found in Kribus (1991).

The matrix eigenvalue problem (6) is much larger than those found in separable linear stability studies, since two directions have to be treated numerically. The standard QR and QZ algorithms have limited applicability here, because their computation time depends cubically on the size of the matrix. We use instead vector-iteration methods: the Generalized Inverse Iteration (Kribus 1990, 1991), and a variant of the Goldhirsch Integration (Goldhirsch, Orszag & Maulik 1987; Kribus 1991). These have the advantage of working with a small number of vectors, trying to isolate a small set of leading eigenvalues, rather than finding the entire eigenvalue spectrum as QR does. This can lead to significant savings in computation time. These iterative methods perform best when used with sparse matrices, such as those derived from a finite-difference discretization of (5). A short account of these methods is included in the Appendix; a full description, convergence tests and code validation are described in Kribus (1991).

4. Stability on the columnar branches

When the base flow is columnar, the linear stability problem (5) becomes separable and the perturbation can be treated numerically in the r-direction only. We can then avoid the complex algorithms designed for more general non-separable cases, and use more efficient methods. We used the spectral code of Yang (1990), applied to problem (5) with a perturbation of the form: $Q = q(r)\,\mathrm{e}^{\sigma t + \mathrm{i}m\theta + \mathrm{i}\varpi z}$. Here the fundamental period of the base flow is infinite, so ϖ may be any real number: κ therefore is redundant and we set it to zero.

The Burgers vortex is stable to inviscid axisymmetric perturbations for all A (L&K). The Leibovich & Stewartson (1983) criterion and computation of the leading eigenvalues show that the same applies to non-axisymmetric perturbations. We conclude that this primary columnar flow is stable to inviscid perturbations. L&K showed that the secondary columnar branch, in the neighbourhood of the bifurcation point, is also stable to inviscid axisymmetric perturbations. The Howard & Gupta (1962) and Leibovich & Stewartson criteria on this branch imply stability to axisymmetric perturbations for $\eta > -0.38$, and instability to non-axisymmetric perturbations for $\eta < -0.08$ (see Kribus 1991).

The leading growth rates are presented in table 1 and figure 4 for several columnar flows on the $\eta < 0$ side of the principal conjugate branch. Solutions on the $\eta > 0$ side are stable, and are not presented. The most unstable mode found is $\varpi = m = -1$, and positive growth rate appears first at $\eta < -0.05$, similar to the prediction of the L&S criterion. We conclude that the secondary columnar branch is unstable to non-axisymmetric perturbations for $\eta < -0.05$, and stable otherwise.

The instability found for the secondary columnar branch is not necessarily generic to this kind of flow. Another choice for the initial vortex will lead to different flows on the secondary columnar branch, which may be less (or more) prone to instability.

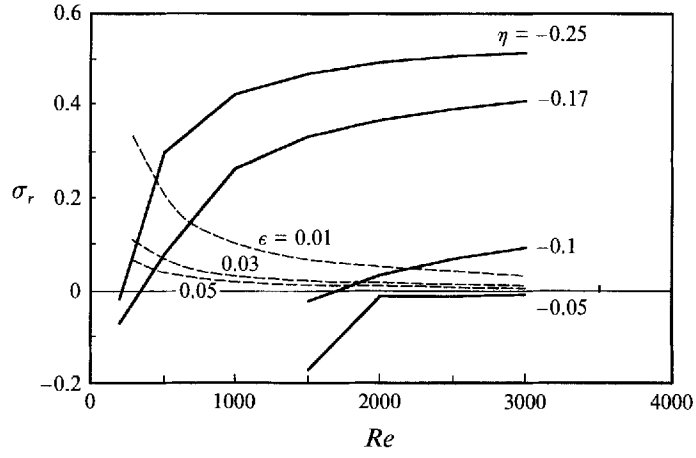

FIGURE 4. Growth rates for the secondary columnar flows. Solid lines are the computed growth rates; dashed lines are $1/(\epsilon Re)$, where ϵ is the initial perturbation amplitude in the range 0.01–0.05. Instability is inferred for growth rates above the dashed lines.

Re	$\eta = -0.05$	$\eta = -0.10$	$\eta = -0.17$	$\eta = -0.25$
200			−0.071+0.456i	−0.018+3.158i
500			0.081+3.858i	0.298+3.175i
1000			0.262+3.879i	0.425+3.175i
1500	−0.171 −3.869i	−0.020+4.755i	0.332+3.885i	0.469+3.173i
2000	−0.013 −3.969i	0.034+4.764i	0.369+3.887i	0.492+3.171i
2500	−0.011 −3.970i	0.070+4770i	0.392+3888i	0.506+3.170i
3000	−0.009 −3.970i	0.095+4.775i	0.408+3.889i	0.514+3.169i

TABLE 1. Leading growth rates for the secondary columnar flows, $\alpha = 14$. All modes with $m = \varpi = -1$

5. Stability on the periodic $k = 1$ branch

We have presented the linear stability problem in a general form, but for applications to vortex breakdown (see Leibovich 1984) we are primarily interested in perturbations that are localized axially and have significant magnitude near the wave centre $z = 0$, but not upstream. We therefore limit our calculations here to the case $\kappa = 0$, which allows the perturbation to be small and non-oscillating upstream of the wave.

We have computed the leading growth rates for several wave amplitudes corresponding to the $k = 1$, $\eta > 0$ branch of figure 1. These amplitudes, measured by $w'(0,0)$, are large, although not large enough to cause flow reversal. Table 2 and figure 5 present the leading growth rates, for values of *Re* where the transition to positive growth rate occurs. The wavy branches with $\eta < 0$, on the other side of μ, bifurcate from the principal conjugate branch, which is already unstable at that point; the stability of these flows is therefore not considered. The $\alpha = 5$ case was selected such that the maximum axial deceleration, $w'(0,0)$, is the same as for the $\alpha = 3$, $\eta = 0.05$ flow. Modes of azimuthal wavenumber in the range $[-2, 2]$ were considered. All $m = 0$ modes have negative growth rates. The $|m| = 1$ modes have the largest growth rate in all cases. Modes $|m| = 2$ also have positive growth rates at large *Re*, but much smaller than for $|m| = 1$. Positive and negative wavenumbers produce eigenvalues and eigenvectors that are complex conjugates of each other, and have the same growth rate.

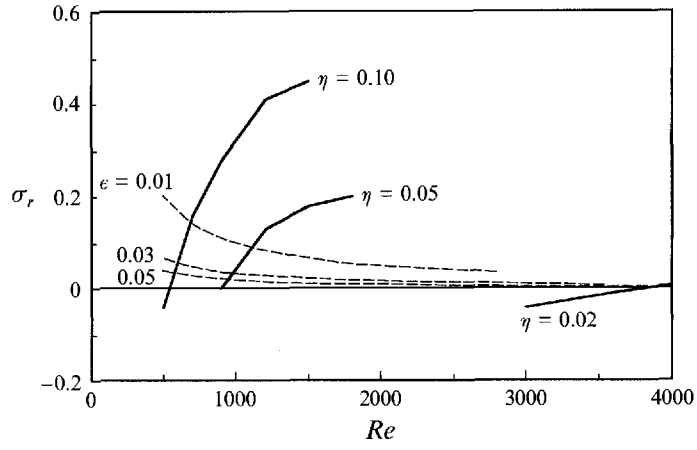

FIGURE 5. As in figure 4, but for cnoidal waves on the $\alpha = 3$, $L = 2$, $k = 1$ branch.

	$\alpha = 3$			$\alpha = 5$
Re	$\eta = 0.02$	$\eta = 0.05$	$\eta = 0.10$	$\eta = 0.078$
500			−0.04 −0.36i	
700			0.16 −0.33i	
900		0.00 −0.39i	0.28 −0.33i	
1200		0.13 −0.35i	0.41 −0.36i	0.00+0.91i
1500		0.18 −0.32i	0.45 −0.43i	0.06+0.29i
1800		0.20 −0.32i		0.11+0.31i
2100				0.14+0.32i
2400				0.17+0.33i
3000	−0.04 −0.52i			
3600	−0.01 −0.51i			
4000	0.01 −0.50i			

TABLE 2. Leading eigenvalues for the wave flows: $\kappa = 0$, $\mu = -1$

Owing to the numerical limitations discussed above, we had to settle for a small value of the radial scaling parameter: $\alpha = 3$, rather than the value $\alpha = 14$ which provides a good fit for experimental velocity profiles upstream of the wave. To estimate the effect of α on the linear stability problem, we compare the leading growth rates for two wave flows having the same maximum axial deceleration (i.e. the same wave 'amplitude'): $\alpha = 3$, $\eta = 0.05$ and $\alpha = 5$, $\eta = 0.078$. The qualitative dependence on *Re* seems similar for both cases (see figure 6), except that the onset of instability is shifted to higher values of *Re*. The leading eigenfunctions corresponding to $\alpha = 5$ are also qualitatively similar to the $\alpha = 3$ counterparts. If this qualitative similarity exists also for higher α (which are not accessible to current computational tools), then the conclusions drawn here for small α should carry over, possibly with some modifications, to more realistic models of physical vortex flows.

The direction of rotation (positive or negative θ) of flow structures is determined by the signs of the imaginary part of the eigenvalue, σ_i, and the azimuthal wavenumber m. All cases in table 2 have $m = -1$, but the sign of σ_i is different for $\alpha = 3$ and 5. The leading mode for $\alpha = 3$ rotates in the negative θ-direction, opposite to the base-flow azimuthal velocity; for $\alpha = 5$, the direction is reversed; and there should be some value

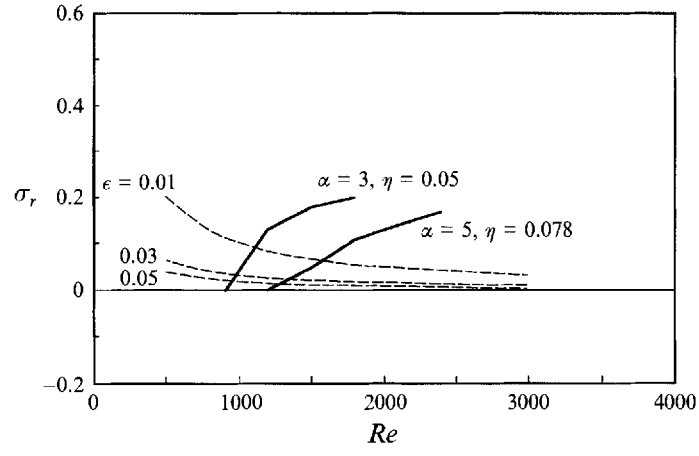

FIGURE 6. Comparison of leading growth rates between $\alpha = 3$, $\eta = 0.05$ and $\alpha = 5$, $\eta = 0.078$ flows. The amplitude of the basic nonlinear wave in these two cases is the same.

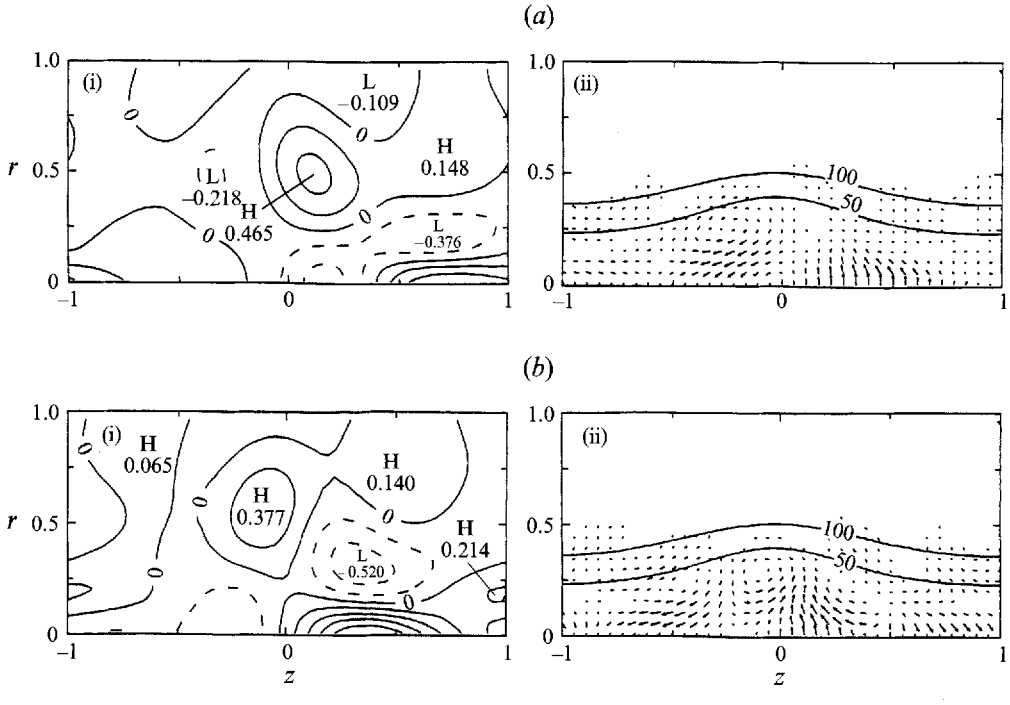

FIGURE 7. (*a*) Real part and (*b*) imaginary part of the velocity field of the leading mode for $\alpha = 3$, $L = 2$, $k = 1$, $\eta = 0.10$, $Re = 500$ flow. (i) Contour plot of the azimuthal velocity component. (ii) Arrows show the projection of velocity onto the meridional plane. Representative streamlines of the base flow are also shown.

of α in-between, where the perturbation does not rotate at all (standing wave). The complex-conjugate case ($m = 1$) yields the same results since m and σ_i change sign simultaneously. It seems then that the rotation of the perturbation flow field depends on the details of the base flow, and is not correlated solely with the direction of the base-flow azimuthal velocity component. Flow structures in spiral-type vortex

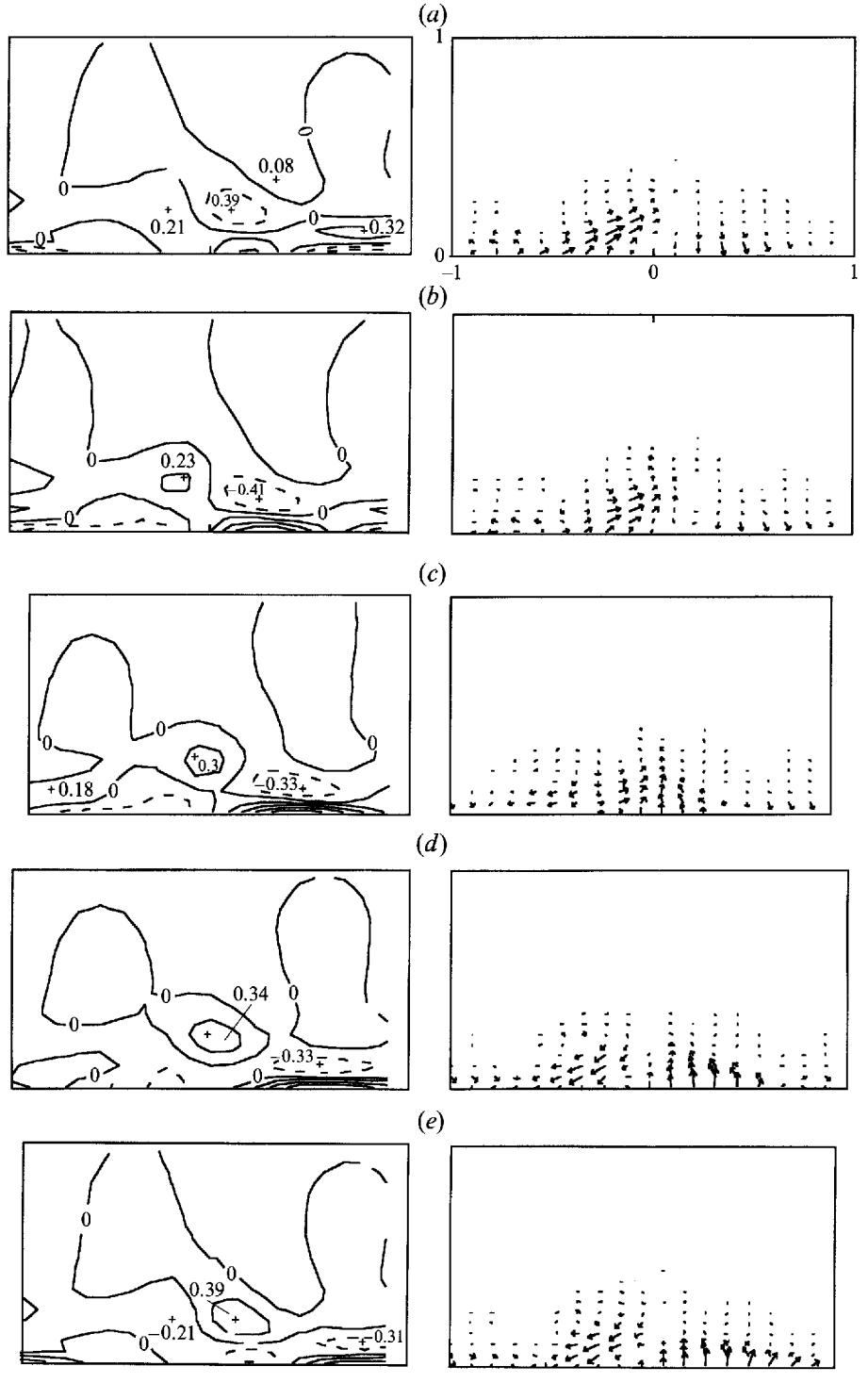

FIGURE 8. Evolution of the perturbation velocity field at several phase values: (*a*) 0, (*b*) $\pi/4$, (*c*) $\pi/2$, (*d*) $3\pi/4$, (*e*) π. Contour plots are of the azimuthal velocity component; the arrow plots are the projection of the velocity onto the meridional plane.

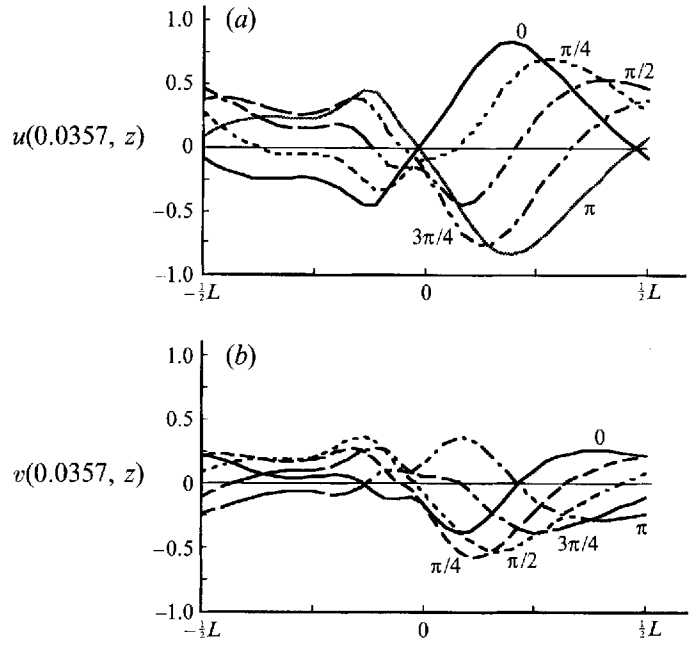

FIGURE 9. Perturbation velocity profiles along the axis, at $r = 0.036$, at several phase stations. (*a*) Radial velocity u, (*b*) azimuthal velocity v.

breakdown usually rotate in the same direction as the upstream azimuthal velocity (Leibovich 1984). The upstream flow in these experiments correspond to higher values of α than considered here; this is consistent with the trend demonstrated by the two values of α presented here.

Figure 7 shows the velocity fields of the most unstable mode for $\alpha = 3$, $L = 2$, $\eta = 0.10$, $Re = 500$. As mentioned above, the velocity fields for the $\alpha = 5$ case are qualitatively similar. The eigenfunctions are normalized such that $\max(u, v, w) = 1$.

The perturbation velocity field contains large values and large gradients in the 'wave region' and downstream, but reverts to smaller values and almost columnar behaviour upstream ($z < 0$). The distinction between the upstream and downstream sides of the wave region is likely to be even more pronounced if the computation is repeated for larger values of L. Figure 8 shows the evolution the velocity field for the case in figure 7, at several values of the phase $(\sigma_i t + m\theta)$; these may be interpreted as different azimuthal stations or different times in a fixed azimuthal position. In figure 8, the contour plots display the perturbation azimuthal velocity, and the arrow plots the projection of the velocity vector onto the meridional plane. The large flow structures (seen as 'rolls' or 'azimuthal jets' in the velocity plots) seem to oscillate and propagate axially between the wave centre $z = 0$ and the downstream side. Faler & Leibovich (1978) found similar features in their measurements of velocities in a bubble-type breakdown: velocities oscillate strongly (both in time and in r) near the axis inside the 'bubble' and at the downstream side, but not upstream.

Figure 8 contains a large amount of information, describing three velocity components as a function of three coordinates (r, z and phase). Figure 9 presents cross-sections through these data, showing typical variations of individual velocity components along the axial direction, at several values of the phase. It is easy to identify the nearly columnar region with small-magnitude perturbations upstream of

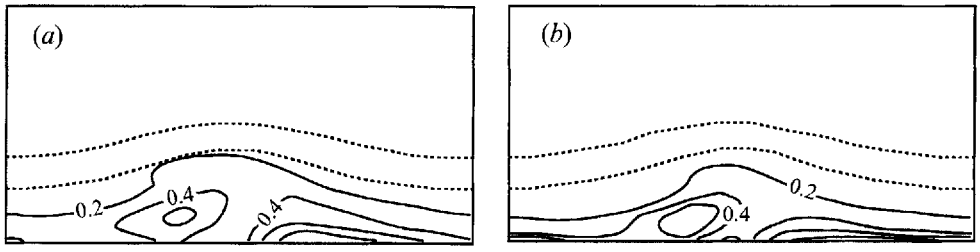

FIGURE 10. Absolute magnitude of the complex perturbation velocity (solid lines), and representative streamlines of the base flow (dotted lines); $a = 3$, $L = 2$, $h = 0.10$. (*a*) $Re = 500$, (*b*) $Re = 1500$.

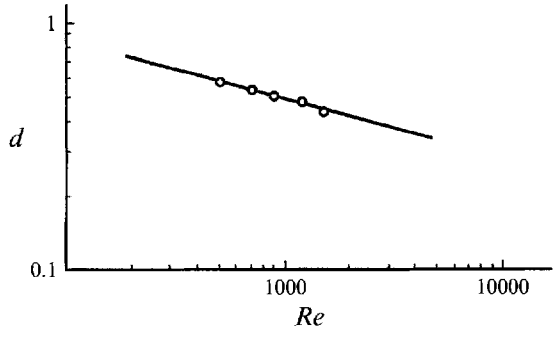

FIGURE 11. The radial lengthscale d of the leading mode, $\alpha = 3$, $\eta = 0.10$.

the wave ($z < 0$). Downstream of the wave centre, the perturbation velocity resembles half a period of a wave with axial wavenumber $\varpi = -1$, which propagates upstream (when we consider a constant-θ plane) and coming to rest near $z = 0$.

The downstream side of the leading mode has significant radial velocity near the axis, producing 'sloshing' motions across the axis. Garg & Leibovich (1979) and others have observed that the rear end of a bubble-type breakdown contains significant low-frequency oscillations, which seem to carry fluid across the axis, and found the frequency to be consistent with $|m| = 1$ wavenumber. The upstream side of the bubble does not contain such oscillations, which is also consistent with the instability described here.

The absolute magnitude of the complex perturbation velocity, $(|u|^2 + |v|^2 + |w|^2)^{\frac{1}{2}}$, is presented in figure 10. The perturbations are largest at the wave centre and downstream near the axis. The values are normalized such that the highest value is 1.

All three components of the velocity are small near the wall, and the radial extent of non-negligible velocity is somewhat smaller for large Re. This suggests the behaviour of a centre-mode, although the Reynolds numbers considered here may not be large enough to estimate the limiting behaviour at $Re \to \infty$. Let d be a measure of radial lengthscale of the unstable mode, defined by $(u^2 + w^2)^{\frac{1}{2}} > 0.2$ for $r \leqslant d$. In figure 11 we plot d against Re, with a good fit to the line: $d \propto Re^{-0.24}$. This may be a useful guide in developing a centre-mode-type analysis of the inviscid limit. This behaviour of the unstable modes signifies that the location of the wall (related to the choice of α) and the type of boundary condition applied at the wall may not have a significant effect on the solution for the leading mode.

6. Conclusions

We have shown that large-amplitude wavetrains and solitary waves in vortices are stable to axisymmetric disturbances, and are unstable to bending modes provided the wave amplitude exceeds a critical threshold. The instability is confined to regions near the vortex axis and downstream of the point of maximum reduction of axial velocity in the wave. The radial extent of the most unstable perturbation is reduced when increasing the Reynolds number; the perturbation is therefore sensibly describable as a 'centre mode'. Laser Doppler anemometer measurements (Faler & Leibovich 1978) support flow visualizations that show that the velocity fluctuations are largest in the downstream third of the bubble form of vortex breakdown. If the recirculation region of a vortex breakdown may be identified as a large-amplitude axisymmetric wave, then the instability to bending modes, and the location of the maximum instability strength, are all consistent with experimental evidence. The instabilities demonstrated theoretically here are therefore consistent with the suggestions made by Leibovich (1983, 1984) and by Maxworthy, Mory & Hopfinger (1983).

Our stability calculations show that perturbations with azimuthal wavenumber $m = \pm 1$ are most unstable, and therefore presumably preferred. This is consistent with the experimental findings of Garg & Leibovich (1979).

In addition, the stability results show that the sense of rotation of the pattern associated with the most unstable perturbation is not always the same, but rather depends on the parameters of the basic flow. The literature (see Leibovich 1984 for a review) reports differing senses of rotation of streaklines. While this can mislead inferences about velocity fields, the results here are clear that a single rotation sense is not to be expected for all flows. Furthermore, the present results show that steady (i.e. non-rotating) non-axisymmetric patterns can be expected. This, too, has been demonstrated experimentally by Sarpkaya (1971) and by Faler & Leibovich (1977).

This work was supported by the US Air Force Office of Scientific Research, under grants AFOSR-89-0346 and AFOSR-91-0226.

Appendix. Computing leading eigenvalues

Traditional methods for solving a matrix eigenvalue problem such as (6) usually involve finding all the eigenvalues, using the QZ algorithm (e.g. from IMSL or Eispack) and then sorting by the real part to find the leading eigenvalues. This involves $O(n^3)$ work, where n is the order of the matrices, and becomes expensive or impractical for large n; little or no advantage can be taken of sparsity or other structure of $\boldsymbol{A}$ and $\boldsymbol{B}$. More economical methods exist for extracting selected eigenvalues and eigenvectors of standard eigenvalue problems, i.e. when $\boldsymbol{B}$ is invertible, such as power and Lanczos methods. These methods select eigenvalues according to their absolute magnitude, and are therefore not directly applicable to stability problems.

Goldhirsch *et al.* (1987) presented a method for computing the leading eigenvalues of a standard eigenvalue problem, involving integration of a transient problem derived from (6) when $\boldsymbol{B}$ is invertible. This method originally included a pre-filtering stage followed by an Arnoldi-type process to approximate the leading invariant subspace. The length of the filtering stage is somewhat arbitrary; in addition, convergence may become very slow if the separation of the eigenvalues is small. Another problem may arise if the problem is defective, i.e. a leading eigenvalue has generalized eigenvectors; in this case, the integration method may return inconclusive or inconsistent results.

We have modified the integration procedure by removing the initial filtering and constructing the approximate invariant subspace by Simultaneous Iterations using Schur vectors (Stewart 1976). This ensures convergence to a meaningful solution even for defective matrices, and resolves the problem of possibly inadequate or excessive filtering time. $\boldsymbol{B}$ in (6) is not invertible, and some matrix manipulation (analogous to using an equation for the pressure) was required to reduce (6) to standard eigenvalue problem form (see Kribus 1991). We found that as the matrix size increased due to application of finer grids, convergence of this method slowed considerably; it turns out that more and more eigenvalues appeared with growth rate close to that of the leading eigenvalue. We were able therefore to use this method only on low-resolution grids (e.g. 30×30), to obtain low-accuracy approximate leading eigenvalues. These coarse-grid solutions were then used as initial guesses for the procedure described next, which demonstrated very fast convergence if supplied with a good initial guess.

Kribus (1990) suggested the Generalization Inverse Iteration (GII), which applies to a problem like (6) the linear fractional transformation

$$\sigma = \beta + \alpha \frac{\lambda - 1}{\lambda + 1}; \tag{A 1}$$

α is a real positive, and β a complex, constant. The important effect of (A 1) is to map the half-plane to the left of $\sigma = \beta$ to the inside of the unit circle in the λ-plane. If we select β such that, for some m,

$$\mathrm{Re}(\sigma_i) \begin{cases} > \mathrm{Re}(\beta), & i = 1 \ldots m, \\ < \mathrm{Re}(\beta), & i = m+1 \ldots n, \end{cases}$$

then the corresponding m eigenvalues in the λ-plane will be *dominant*:

$$|\lambda_i| \begin{cases} > 1, & i = 1 \ldots m, \\ < 1, & i = m+1 \ldots n. \end{cases}$$

The eigenvalue problem for λ is of standard form:

$$\boldsymbol{C}\boldsymbol{u} \equiv \boldsymbol{C}_1^{-1}\boldsymbol{C}_2\boldsymbol{u} = \lambda \boldsymbol{u}, \tag{A 2}$$

where $$\boldsymbol{C}_1 = -[\boldsymbol{A} - (\alpha + \beta)\boldsymbol{B}], \quad \boldsymbol{C}_2 = [\boldsymbol{A} + (\alpha - \beta)\boldsymbol{B}].$$

The problem of computing the leading eigenvalues of (6) becomes that of computing the dominant eigenvalues of (A 2); the standard methods can now be applied. We used a generalization of the power method, Simultaneous Iteration, to find dominant eigenvalues and invariant spaces of $\boldsymbol{C}$. The leading eigenvalues of (6) can then be recovered by inverting (A 1); eigenvectors for the σ and λ problems are identical.

The mapping constants α and β allow the user some control over the rate of convergence and the order in which the leading eigenvalues emerge during the iteration. The user must have an estimate of where in the complex plane the leading eigenvalues reside; β is set to the left of this region. The point $c = \beta + \alpha$ is a singular point of (A 1) which maps to infinity in the λ-plaque; eigenvalues close to c will map to very large modulus in the λ-plane, and will converge rapidly during the iteration of (A 2). α should be set, therefore, so that c is near the centre of the leading region or near the most important eigenvalue. A more detailed discussion of the mapping (A 1) and examples of its use may be found in Kribus (1990, 1991). In the present application, coarse-grid solutions were available from the integration scheme; with a good choice of α and β, convergence on finer grids could be reached within a few (< 10)

GII steps. We were limited in problem size only by the linear solver (ME28 from the Harwell library) used to perform the multiplication by $\boldsymbol{C}_1^{-1}$ in (A 2); see Kribus 1991 for details and discussion. A more specific solver that would exploit better the specific structure of the matrices in (6) could extend considerably the range of applicability of this algorithm.

REFERENCES

BENJAMIN, T. B. 1962 Theory of the vortex breakdown phenomenon. *J. Fluid Mech.* **14**, 593–629.

BENJAMIN, T. B. 1967 Some developments in the theory of vortex breakdown. *J. Fluid Mech.* **28**, 65–84.

BENJAMIN, T. B. 1972 The stability of solitary waves. *Proc. R. Soc. Lond.* A **328**, 153–183.

BENJAMIN, T. B. 1974 Lectures on nonlinear wave motion. In *Nonlinear Wave Motion* (ed. A. C. Newell). Lectures in Applied Mathematics, vol. 15, pp. 3–47. Am. Math. Soc.

BERAN, P. S. 1987 Numerical simulations of trailing vortex bursting. *AIAA Paper* 87–1313.

FALER, J. H. & LEIBOVICH, S. 1977 Disrupted states of vortex flow and vortex breakdown. *Phys. Fluids* **20**, 1385–1400.

FALER, J. H. & LEIBOVICH, S. 1978 An experimental map of the internal structure of a vortex breakdown. *J. Fluid Mech.* **86**, 313–335.

GARG, A. K. & LEIBOVICH, S. 1979 Spectral characteristics of vortex breakdown flow fields. *Phys. Fluids* **22**, 2053–2064.

GOLDHIRSCH, I., ORSZAG, S. A. & MAULIK, K. 1987 An efficient method for computing leading eigenvalues and eigenvectors of large asymmetric matrices. *J. Sci. Comput.* **2**, 33–58.

HAFEZ, M., KURUVILA, G. & SALAS, M. D. 1986 Numerical study of vortex breakdown. *Appl. Numer. Maths* **2**, 291–302.

HOWARD, L. & GUPTA, A. S. 1962 On the hydrodynamic and hydromagnetic stability of swirling flows. *J. Fluid Mech.* **14**, 463–476.

KRIBUS, A. 1990 Computation of leading eigenspaces for generalized eigenvalue problems. *Trans. Seventh Army Conf. on Applied Mathematics and Computing*, ARO 90–1.

KRIBUS, A. 1991 Large-amplitude waves, instabilities, and breakdown in vortex flows. PhD thesis, Cornell University.

LEIBOVICH, S. 1970 Weakly nonlinear waves in rotating fluids. *J. Fluid Mech.* **42**, 803–822.

LEIBOVICH, S. 1978 The structure of vortex breakdown. *Ann. Rev. Fluid Mech.* **10**, 221–246.

LEIBOVICH, S. 1983 Vortex stability and breakdown. In *Aerodynamics of Vortical Type Flows in Three Dimensions* (ed. A. D. Young). *AGARD Conf. Proc.* 342 (NATO), *Paper* 23.

LEIBOVICH, S. 1984 Vortex stability and breakdown: Survey and extension. *AIAA J.* **22**, 1192–1206.

LEIBOVICH, S. 1990 Vortex breakdown: A coherent transition trigger in concentrated vortices. In *Turbulence and Coherent Structures* (ed. M. Lesieur & O. Métais), pp. 285–302. Kluwer.

LEIBOVICH, S. & KRIBUS, A. 1990 Large-amplitude wavetrains and solitary waves in vortices. *J. Fluid Mech.* **216**, 459–504 (referred to herein as L&K).

LEIBOVICH, S. & STEWARTSON, K. 1983 A sufficient condition for the instability of columnar vortices. *J. Fluid Mech.* **126**, 335–356.

MAC GIOLLA MHUIRIS, N. 1986*a* Numerical calculations of the stability of some axisymmetric flows proposed as a model for vortex breakdown. PhD thesis, Cornell University.

MAC GIOLLA MHUIRIS, N. 1986*b* Calculations of the stability of some axisymmetric flows proposed as a model of vortex breakdown. *Appl. Numer. Maths* **2**, 273–290.

MAXWORTHY, T., HOPFINGER, E. J. & REDEKOPP, L. G. 1985 Wave motions on vortex cores. *J. Fluid Mech.* **151**, 141–165.

MAXWORTHY, T., MORY, M. & HOPFINGER, E. J. 1983 Waves on vortex cores and their relation to vortex breakdown. In *Aerodynamics of Vortical Type Flows in Three Dimensions* (ed. A. D. Young). *AGARD Conf. Proc.* 342 (NATO), *Paper* 29.

PRESS, W. H., FLANNERY, B. P., TEUKOLSKY, S. A. & VETTERLING, W. T. 1986 *Numerical Recipes, the Art of Scientific Computing*. Cambridge University Press.

PRITCHARD, W. G. 1970 Solitary waves in rotating fluids. *J. Fluid Mech.* **42**, 61–83.

SALAS, M. D. & KURUVILA, G. 1989 Vortex breakdown simulation: a circumspect study of the steady, laminar, axisymmetric model. *Computers & Fluids* **17**, 247–262.

SARPKAYA, T. 1971 On stationary and travelling vortex breakdowns. *J. Fluid Mech.* **45**, 545–559.

STEWART, G. W. 1976 Simultaneous iterations for computing invariant subspaces of non-hermitian matrices. *Numer. Maths* **25**, 123–136.

TA'ASAN, S. 1986 Multigrid method for a vortex breakdown simulation. *Appl. Numer. Maths* **2**, 303–311.

YANG, Z. 1990 Two theoretical studies of stability of swirling flows. PhD thesis, Cornell University.